Optimal Impulsive Closed-Form Control for Spacecraft Formation Flying and Rendezvous

Lucas Riggi and Simone D'Amico

Abstract – **This paper addresses the design of novel optimal closed-form multi-impulsive maneuvers for satellite formation-flying and rendezvous. A new method to derive the state transition matrix for the relative motion in J_2-perturbed eccentric orbits is shown and used to compute (semi-)analytical solutions for formation control. In addition, a delta-v lower bound for eccentric orbits is formulated which provides direct insight into the optimality of the control solutions. The functionality and performance of the resulting maneuvering schemes are numerically analyzed through comparisons with state-of-the-art optimal control. The results of this paper show how closed-form maneuver solutions have the potential to fulfil the requirements posed by future distributed space systems at a fraction of the computational cost and overall complexity.**

I. Introduction

FORMATION-flying and rendezvous are key areas of research in modern spacecraft dynamics, navigation and control. Future distributed space systems (DSS) require the capability to control the relative motion between multiple spacecraft subject to ever more challenging requirements. These involve efficiency (on-board resources), autonomy (no or minimal ground-in-the-loop), and operational constraints (interference with payload, predictability) [1]. This work tries to fulfil the requirements posed by future DSS through the generalization and extension of simple closed-form solutions of the relative spacecraft dynamics.

Previous research done by the authors has led to two flight demonstrations of autonomous formation keeping and reconfiguration, namely in the German TanDEM-X and Swedish PRISMA missions [2-3]. In addition, the relevant findings are being applied in the frame of upcoming on-orbit servicing missions (e.g., US mSTAR [1], German DEOS [4], German FireBird [5]). This paper builds on these results and improves the state-of-the-art by deriving optimal closed-form solutions for formation control in two relevant cases not available in literature, namely in 1) near-circular J_2-perturbed orbits, and 2) unperturbed eccentric orbits.

Several formation control algorithms have been described in the literature. So far, the solutions differ in their range of applicability (elliptical or near-circular orbits), their accuracy (inclusion of perturbations) and their mathematical approach (analytical or numerical). Tillerson et al. [6-7] proposed a fuel-optimal formation control algorithm based on convex optimization techniques. However, it only partially takes into account perturbations. Roscoe et al. [8] designed an optimal algorithm for elliptical perturbed orbits based on Pontryagin's optimal control and Lawden's primer vector theory [9]. This algorithm uses a discretization of the continuous-time optimal control problem and makes the discrete-time optimal maneuver times converge towards the continuous-time truly optimal ones. The issue is that it involves an iterative process that depends on a good initial guess and the algorithm can yield large computational loads. Rogers et al. also uses linear optimal control to optimize maneuver planning in eccentric orbits [10]. As with most numerical methods, their approach is computationally expensive and therefore not necessarily the best solutions for a satellite onboard implementation. A closed-form solution for formation reconfiguration in elliptical orbit has been derived by Schaub [11-12]. However, perturbations are not taken into account and little to no considerations on optimality are made. Gaias and D'Amico [13-14] have designed a formation maneuvering scheme where perturbations are included through a layered approach in a global guidance problem. The resulting required changes of relative orbit elements (ROE) [15] are treated as several local control problems in which the impulsive maneuvers are computed in closed-form neglecting perturbations. Vaddi et al. [16] derived fuel-optimal impulsive solutions for formation reconfiguration, but they are all limited to near-circular orbits with no perturbations taken into account.

This paper offers five main contributions to the state-of-the-art. First of all, a new simple method to derive the state transition matrix (STM) for mean ROE in perturbed orbits of arbitrary eccentricity is derived. The resulting STM is characterized by unprecedented simplicity as compared with other solutions available in literature [17]. Second, this paper extends the well-known three-impulse optimal in-plane ROE reconfiguration solution [13-14] to J_2-perturbed near-circular orbits. Perturbations included are limited to the secular effects, while short-period variations are neglected. Third, a semi-analytical optimal solution for formation reconfiguration in unperturbed eccentric orbits is derived. Fourth, a delta-v lower bound for formation reconfiguration in eccentric orbits is found, which provides the absolute minimum necessary fuel cost for any given reconfiguration. Finally, the optimality of the solutions are numerically verified by comparing the costs achieved by the closed-form solutions with an optimal control algorithm based on primer vector theory [8].

II. Relative Motion Dynamics for Formation Flying

This section describes the relative dynamics of a deputy with respect to a chief spacecraft in J_2-perturbed eccentric orbits. A new STM is derived in mean ROE-space including secular perturbations due to J_2 effects. Step-wise simplifications are later made to conveniently describe the relative dynamics in near-circular orbits or non-perturbed eccentric orbits.

A. J_2-Perturbed Relative Dynamics

The motion of the deputy relative to the chief satellite is described using the set of ROE introduced by D'Amico [15]

L. Riggi is a graduate student with the Department of Aeronautics and Astronautics at Stanford University, Stanford, CA 94305 USA (phone: 650-862-9426; e-mail: lriggi@stanford.edu).

S. D'Amico is an Assistant Professor with the Department of Aeronautics and Astronautics at Stanford University, Stanford, CA 94305 USA (phone: 650-497-4682; e-mail: damicos@stanford.edu).

$$\delta\boldsymbol{\alpha} = \begin{pmatrix} \delta a \\ \delta\lambda \\ \delta e_x \\ \delta e_y \\ \delta i_x \\ \delta i_y \end{pmatrix} = \begin{pmatrix} (a_\mathrm{d} - a_\mathrm{c})/a_\mathrm{c} \\ u_\mathrm{d} - u_\mathrm{c} + (\Omega_\mathrm{d} - \Omega_\mathrm{c})\cos i_\mathrm{c} \\ e_\mathrm{d}\cos\omega_\mathrm{d} - e_\mathrm{c}\cos\omega_\mathrm{c} \\ e_\mathrm{d}\sin\omega_\mathrm{d} - e_\mathrm{c}\sin\omega_\mathrm{c} \\ i_\mathrm{d} - i_\mathrm{c} \\ (\Omega_\mathrm{d} - \Omega_\mathrm{c})\sin i_\mathrm{c} \end{pmatrix}, \quad (1)$$

where the subscripts *c* and *d* denote quantities of the chief and deputy spacecraft respectively. The classical Keplerian orbit elements are denoted by $a, e, i, \Omega, \omega, M$, and mean argument of latitude is $u = M + \omega$. The so-called in-plane ROE, δa, $\delta\lambda$, $\delta\boldsymbol{e}$, correspond to the relative semi-major axis, relative mean longitude, and relative eccentricity vector, whereas the so-called out-of-plane ROE, $\delta\boldsymbol{i}$, is the relative inclination vector. The state of choice is non-singular for circular orbits ($e_\mathrm{c} = 0$), but still singular for equatorial orbits ($i_\mathrm{c} = 0$). Similar to Gaias et al. [18], the secular perturbations caused by J_2 on the individual orbit elements can be incorporated as

$$\delta\dot{\boldsymbol{\alpha}} = \gamma\sum_{i=c,d} k_i \frac{1}{a_i^{7/2}\eta_i^4} \begin{pmatrix} 0 \\ (1+\eta_i)(3\cos^2 i_i - 1) \\ -e_{\mathrm{y},i}(5\cos^2 i_i - 1) \\ e_{\mathrm{x},i}(5\cos^2 i_i - 1) \\ 0 \\ -2\sin i_i \cos i_i \end{pmatrix} = \gamma\sum_{i=c,d} k_i \boldsymbol{f}_i(\delta\boldsymbol{\alpha}, \boldsymbol{\alpha}_c)\,, \quad (2)$$

where

$$\gamma = \frac{J_2}{2}\left(\frac{R_\mathrm{e}}{a_\mathrm{c}}\right)^2 \frac{1}{\eta_c^4}, \eta_i = \sqrt{1 - e_i^2}, k_{d,c} = \pm 1, n = \frac{\sqrt{\mu}}{{a_c}^{3/2}}, \kappa_i = \frac{2\gamma}{3\eta}\frac{1}{a_i^{7/2}\eta_i^4}\,. \quad (3)$$

For small ROE as defined by (1), $\delta\dot{\boldsymbol{\alpha}}$ can be expanded about the chief (reference) orbit to first order using a Taylor expansion

$$\delta\dot{\boldsymbol{\alpha}} = \gamma\sum_{i=c,d} k_i \boldsymbol{f}_i(\delta\boldsymbol{\alpha}, \boldsymbol{\alpha}_c) \approx \gamma\frac{\partial f_d}{\partial\delta\alpha}\Big|_{\delta\boldsymbol{\alpha}=\boldsymbol{0}}\delta\boldsymbol{\alpha} = \boldsymbol{A}_{\boldsymbol{J_2}}\delta\boldsymbol{\alpha}\,, \quad (4)$$

where $\boldsymbol{A}_{\boldsymbol{J_2}}$ is the contribution to the system (or plant) matrix due to J_2 only. Including un-perturbed Keplerian dynamics, the full system matrix becomes

$$\boldsymbol{A} = \boldsymbol{A}_{\boldsymbol{K}} + \boldsymbol{A}_{\boldsymbol{J_2}} = \frac{3}{2}\kappa n \begin{pmatrix} 0 & 0 & 0 & 0 & 0 & 0 \\ -\frac{7}{2}MQ - \frac{1}{\kappa} & 0 & e_x GHQ & e_y GHQ & -GS & 0 \\ \frac{7}{2}e_y P & 0 & -4e_x e_y HP & -(1+4e_y^2 H)P & 5e_y S & 0 \\ -\frac{7}{2}e_x P & 0 & (1+4e_x^2 H)P & 4e_x e_y HP & -5e_x S & 0 \\ 0 & 0 & 0 & 0 & 0 & 0 \\ \frac{7}{2}S & 0 & -4e_x HS & -4e_y HS & 2T & 0 \end{pmatrix}, \quad (5)$$

where the subscript *c* has been dropped and

$$P = (5\cos^2 i - 1), Q = (3\cos^2 i - 1), R = \sin 2i, S = \sin^2 i\,, \quad (6)$$

$$M = 1 + \eta, G = 4 + 3\eta, H = \frac{1}{\eta^2}\,, \quad (7)$$

are constant coefficients which depend on i and e. The only slow time-varying parameter in (5) is the reference argument of perigee. For small step sizes, as encountered in navigation [3], the STM can be approximated as

$$\boldsymbol{\Phi}_{\boldsymbol{2,1}} = e^{A(t_2 - t_1)} \approx \boldsymbol{I} + \left(\boldsymbol{A}_{\boldsymbol{K}} + \boldsymbol{A}_{\boldsymbol{J_2}}\right)dt\,. \quad (8)$$

For longer step sizes, as encountered in propagation and maneuver planning, one can directly solve for the integral of the plant matrix through a change of variables to obtain a time-invariant plant [19]. As a consequence, (8) can be derived in closed-form and show a linear trend of all ROE except $\delta\boldsymbol{e}$ which rotates as a harmonic oscillator, and $\delta a, \delta i_x$ which are constants. The full solution of the linearized dynamics of relative motion incorporates an arbitrary number of impulsive delta-v maneuvers during the reconfiguration from $\delta\boldsymbol{\alpha}(t_0) = \delta\boldsymbol{\alpha}_0$ to $\boldsymbol{\alpha}(t_F) = \delta\boldsymbol{\alpha}_F$ as [13]

$$[\boldsymbol{\Phi}_{\mathrm{F},1}\boldsymbol{B}_1, \boldsymbol{\Phi}_{\mathrm{F},2}\boldsymbol{B}_2, \ldots]\boldsymbol{x} = na_\mathrm{c}\left(\delta\boldsymbol{\alpha}_\mathrm{F} - \boldsymbol{\Phi}_{\mathrm{F},0}\delta\boldsymbol{\alpha}_0\right) = [A\ L\ E\ F\ I\ J]^T\,, \quad (9)$$

where $\boldsymbol{B}_i$ is the control input matrix given by the Gauss Variational Equations (GVE) [12] for the i^{th} impulse and $\boldsymbol{x}$ is the vector of all impulsive delta-vs executed by the deputy in the Hill's Radial, Tangential, Normal (RTN) frame. Here, due to the linearization assumptions, mean and osculating orbit elements are assumed identical as used in the GVE. For the rest of this paper, the quantities on the right side of (9) are assumed known from the desired reconfiguration problem.

B. J_2-Perturbed Relative Motion in Near-Circular Orbits

For small eccentricity of the chief (or reference) orbit, the STM can be simplified to [15]

$$\boldsymbol{\Phi}_{\boldsymbol{2,1}} = \begin{pmatrix} 1 & 0 & 0 & 0 & 0 & 0 \\ -\frac{3n}{2N}\Delta u_{2,1} & 1 & 0 & 0 & \frac{\mu}{N}\Delta u_{2,1} & 0 \\ 0 & 0 & \cos(\frac{\varphi}{N}\Delta u_{2,1}) & -\sin(\frac{\varphi}{N}\Delta u_{2,1}) & 0 & 0 \\ 0 & 0 & \sin(\frac{\varphi}{N}\Delta u_{2,1}) & \cos(\frac{\varphi}{N}\Delta u_{2,1}) & 0 & 0 \\ 0 & 0 & 0 & 0 & 1 & 0 \\ 0 & 0 & 0 & 0 & \frac{\lambda}{N}\Delta u_{2,1} & 1 \end{pmatrix}, \quad (10)$$

where $\Delta u_{2,1} = u_2 - u_1$ is the shift of chief's mean argument of latitude and

$$\begin{aligned} \dot{\varphi} &= \tfrac{3}{2}n\gamma(5\cos^2 i - 1) \\ \mu &= -\tfrac{21}{2}n\gamma\sin 2i, \lambda = 3n\gamma\sin^2 i \\ N &= n + \dot{\varphi} + \tfrac{1}{2}\eta\lambda\frac{3\cos^2 i - 1}{\sin^2 i} \end{aligned} \quad (11)$$

The effects of an impulse at a specific mean argument of latitude u are given by the GVE as [15]

$$\Delta\,\delta\boldsymbol{\alpha} = \boldsymbol{B}\boldsymbol{x} = \frac{1}{an}\begin{pmatrix} 0 & 2 & 0 \\ -2 & 0 & 0 \\ \sin u & 2\cos u & 0 \\ -\cos u & 2\sin u & 0 \\ 0 & 0 & \cos u \\ 0 & 0 & \sin u \end{pmatrix}\begin{pmatrix} x_\mathrm{R} \\ x_\mathrm{T} \\ x_\mathrm{N} \end{pmatrix}. \quad (12)$$

It is noteworthy that the effects of out-of-plane maneuvers (N) are fully decoupled from in-plane maneuvers (R-T) due to our choice of ROE.

C. Simplifications for Non-Perturbed Eccentric Orbits

For non-perturbed eccentric orbits it is convenient to replace the relative mean longitude $\delta\lambda$ with a modified state parameter

$$\delta\lambda' = M_d - M_c + \eta[\omega_d - \omega_c + (\Omega_d - \Omega_c)cosi_c] \quad (13)$$

which is referred to as modified relative mean longitude. This choice eliminates the effects of a tangential impulse (T) on the modified relative mean longitude, thus simplifying greatly the dynamics of the reconfiguration. The STM reduces to

$$\boldsymbol{\Phi}_{2,1} = \begin{pmatrix} 1 & 0 & 0 & 0 & 0 & 0 \\ -\frac{3}{2}\Delta M_{2,1} & 1 & 0 & 0 & 0 & 0 \\ 0 & 0 & 1 & 0 & 0 & 0 \\ 0 & 0 & 0 & 1 & 0 & 0 \\ 0 & 0 & 0 & 0 & 1 & 0 \\ 0 & 0 & 0 & 0 & 0 & 1 \end{pmatrix}, \quad (14)$$

and the effects of an impulsive burn executed at a specific true anomaly ν on the ROE are given by [12]

$$\Delta\delta\boldsymbol{\alpha} = \boldsymbol{B}\boldsymbol{x} = \frac{1}{an}\begin{pmatrix} \frac{2}{\eta}e\sin\nu & \frac{2}{\eta}(1+e\cos\nu) & 0 \\ -\frac{2\eta^2}{1+e\cos\nu} & 0 & 0 \\ \eta\sin\theta & \eta\frac{(2+e\cos\nu)\cos\theta+e_x}{1+e\cos\nu} & \frac{\eta e_y}{\tan i}\frac{\sin\theta}{1+e\cos\nu} \\ -\eta\cos\theta & \eta\frac{(2+e\cos\nu)\sin\theta+e_y}{1+e\cos\nu} & \frac{-\eta e_x}{\tan i}\frac{\sin\theta}{1+e\cos\nu} \\ 0 & 0 & \eta\frac{\cos\theta}{1+e\cos\nu} \\ 0 & 0 & \eta\frac{\sin\theta}{1+e\cos\nu} \end{pmatrix}\begin{pmatrix} x_R \\ x_T \\ x_N \end{pmatrix}, \quad (15)$$

where $\theta = \nu + \omega$ is the true argument of latitude of the maneuver.

III. Control in Perturbed Near-Circular Orbits

This section focuses on near-circular chief orbits using the dynamics described by (10-12). The three-impulse tangential optimal solution given by Gaias and D'Amico [13] is extended to the case of perturbed orbits, including secular J_2 effects. Additionally, an optimal impulsive maneuver for perturbed out-of-plane reconfigurations is derived in closed-form.

A. In-Plane Reconfiguration

The following delta-v lower bound for the in-plane ROE reconfiguration in near-circular orbit has been derived from the GVE [13]

$$\delta v_{LB} = \max\left(\tfrac{na}{2}\|\Delta\delta\boldsymbol{e}\|, \tfrac{na}{2}|\Delta\delta a^*|\right), \quad (16)$$

where $|\Delta\delta a^*|$ is the maximum between the aimed direct change in relative semi-major axis and the change in relative semi-major axis that allows a drift in relative mean longitude to accomplish the aimed change in $\delta\lambda$ over the time span of the reconfiguration. If δa_{transf} is the relative semi-major axis needed for the drift to achieve $|\Delta\delta\lambda|$ in the available reconfiguration span Δu_{reconf}, then

$$|\Delta\delta a^*| = \max(|\delta a_F - \delta a_0|, |\delta a_F - \delta a_{\text{transf}}|, |\delta a_{\text{transf}} - \delta a_0|), \quad (17)$$

$$\delta a_{\text{transf}} = \tfrac{2}{3}|\Delta\delta\lambda|/\Delta u_{\text{reconf}}, \quad (18)$$

An immediate consequence of (16), is that the optimal reconfiguration maneuver corresponds to a minimum path problem in the ROE state-space, as illustrated in Fig. 1. If the desired change in the drift coefficient $|\Delta\delta a^*|$ is dominant, the fuel-optimal maneuvers must minimize the reconfiguration path length in the plane $(\delta\lambda, \delta a)$, see Fig. 1 (right). If the change in the shape of the relative orbit $\|\Delta\delta\boldsymbol{e}\|$ is dominant, the optimal maneuvers must minimize the reconfiguration path length in the $\delta\boldsymbol{e}$ plane, see Fig. 1 (left). From (12), if the required change of $\delta\boldsymbol{e}$ is dominant, fuel optimality is guaranteed by three tangential delta-vs separated by half orbit period with the first pulse at $\bar{u}_{\text{ip}} = \text{atan}\left(\frac{\Delta\delta e_y}{\Delta\delta e_x}\right)$, see Fig. 1 [13].

Earth's oblateness J_2 effects induce a rotation of $\delta\boldsymbol{e}$ (Fig. 2) during the reconfiguration time span. The resulting evolution of $\delta\boldsymbol{e}$ with three tangential impulses is given by

$$\boldsymbol{R}_{F,3}\left(\boldsymbol{R}_{3,2}\left(\boldsymbol{R}_{2,1}\left(\boldsymbol{R}_{1,0}\delta\boldsymbol{e}_0 + \Delta\delta\boldsymbol{e}_1\right) + \Delta\delta\boldsymbol{e}_2\right) + \Delta\delta\boldsymbol{e}_3\right) = \delta\boldsymbol{e}_F, \quad (19)$$

where $\boldsymbol{R}_{j,i}$ is the rotation matrix applied to $\delta\boldsymbol{e}$ between u_i and u_j

$$\boldsymbol{R}_{j,i} = \begin{pmatrix} \cos\left[\frac{\dot{\varphi}}{N}(u_j - u_i)\right] & -\sin\left[\frac{\dot{\varphi}}{N}(u_j - u_i)\right] \\ \sin\left[\frac{\dot{\varphi}}{N}(u_j - u_i)\right] & \cos\left[\frac{\dot{\varphi}}{N}(u_j - u_i)\right] \end{pmatrix}, \quad (20)$$

and $\Delta\delta\boldsymbol{e}_i$ is the effect of a tangential burn at a location u_i on $\delta\boldsymbol{e}$ given by (12). Equation (19) can be re-written as

$$\begin{pmatrix}\cos U_1 \\ \sin U_1\end{pmatrix}x_{T1} + \begin{pmatrix}\cos U_2 \\ \sin U_2\end{pmatrix}x_{T2} + \begin{pmatrix}\cos U_3 \\ \sin U_3\end{pmatrix}x_{T3} = \begin{pmatrix}E \\ F\end{pmatrix}, \quad (21)$$

where

$$U_i = (1-c)u_i + cu_F, \quad (22)$$

$$c = \frac{\dot{\varphi}}{N}. \quad (23)$$

Following (21-23), a change of variable is introduced which transfers the effects of J_2 from the equations to the variables. This is highlighted in Table 1 through bold fonts. As a result, the equations of the perturbed and ideal reconfiguration retain the same form and structural solution. In particular the burns have to occur at

$$u_i = (\bar{U} + k_i\pi - cu_F)/(1-c), \quad (24)$$

where $\bar{U} = \text{atan}(\frac{F}{E})$, and the delta-v sizes are given in Tables 2-3. For instance, if $\bar{U} \in [0, \pi/2[$ and $k_i = 0,1,3$ is chosen, then $B = E$, the signs of $\cos(U_i)$ are $(+--)$ and the delta-vs are given by the first line of Table 2.

B. Out-of-Plane Reconfiguration

From (12), it is evident that a single delta-v is necessary and sufficient to achieve the aimed end-condition in the relative inclination vector $\delta\boldsymbol{i}$.

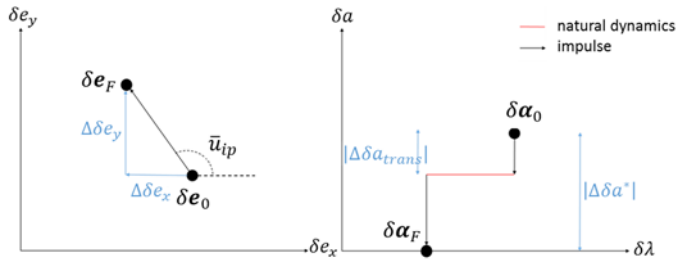

Figure 1. Formation reconfiguration in ROE state-space

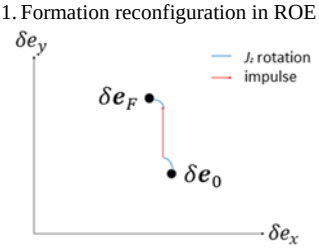

Figure 2. Effect of J_2 on relative eccentricity vector during reconfiguration

TABLE 1. DYNAMICS EQUATIONS OF THE IN-PLANE RECONFIGURATION IN NEAR-CIRCULAR ORBITS

	Perturbed reconfiguration	**Ideal reconfiguration**
Dynamics Equations	$2(x_{T1}+x_{T2}+x_{T3}) = A$ $-3\boldsymbol{q}'x_{T1} - 3\boldsymbol{p}'x_{T2} - 3\boldsymbol{l}'x_{T3} = \boldsymbol{L}'$ $2\cos\boldsymbol{U_1}x_{T1} + 2\cos\boldsymbol{U_2}x_{T2} + 2\cos\boldsymbol{U_3}x_{T3} = E$ $2\sin\boldsymbol{U_1}x_{T1} + 2\sin\boldsymbol{U_2}x_{T2} + 2\sin\boldsymbol{U_3}x_{T3} = F$ (25)	$2(x_{T1}+x_{T2}+x_{T3}) = A$ $-3qx_{T1} - 3px_{T2} - 3lx_{T3} = L$ $2\cos u_1x_{T1} + 2\cos u_2x_{T2} + 2\cos u_3x_{T3} = E$ $2\sin u_1x_{T1} + 2\sin u_2x_{T2} + 2\sin u_3x_{T3} = F$ (26)
Change of variables	$\boldsymbol{q}' = u_F - \frac{U_1}{1-c}$ $\boldsymbol{p}' = u_F - \frac{U_2}{1-c}$ $\boldsymbol{l}' = u_F - \frac{U_3}{1-c}$ (27)	$q = u_F - u_1$ $p = u_F - u_2$ $l = u_F - u_3$ (28)
	$\boldsymbol{U_i} = (1-c)u_i + cu_F$ (29)	u_i
	$\boldsymbol{L}' = \frac{N}{n}L + 3\frac{cu_F}{1-c}A - \frac{\mu}{n}(u_F - u_N)I$ (30)	L

TABLE 2. DELTA-V SOLUTIONS FOR IN-PLANE RECONFIGURATION IN NEAR-CIRCULAR ORBITS

Aimed end-conditions			Choice of k_i	$\tilde{x} = \frac{bA+gB}{4b}$	
	B	b	Signs	+ - -, - - +, - + -	+ - +,+ + -, - + +
$\bar{U} \in [0, \pi/2[$	E	$\cos\bar{U}$	sign($\cos U_i$)	$g = 1$	$g = -1$
$\bar{U} = \pi/2$	F	$\sin\bar{U}$	sign($\sin U_i$)		
$\bar{U} \in]\pi/2, \pi[$	E	$\cos\bar{U}$	sign($\cos U_i$)	$g = -1$	$g = 1$

TABLE 3. DELTA-V COMPUTATION

Signs	$\tilde{x}$	D	Delta-v expressions
+ - - - + +	x_{T1}	$12b(p'-l')$	$x_{T2} = -(4bL' + 3g(q'-l')B + 3b(q'+l')A)/D$ $x_{T3} = +(4bL' + 3g(q'-p')B + 3b(q'+p')A)/D$
- - + + + -	x_{T3}	$12b(q'-p')$	$x_{T1} = -(4bL' - 3g(p'-l')B + 3b(p'+l')A)/D$ $x_{T2} = +(4bL' - 3g(q'-l')B + 3b(q'+l')A)/D$
- + - + - +	x_{T2}	$12b(q'-l')$	$x_{T1} = -(4bL' + 3g(p'-l')B + 3b(p'+l')A)/D$ $x_{T3} = +(4bL' - 3g(q'-p')B + 3b(q'+p')A)/D$

Neglecting perturbations, the location and magnitude of the single cross-track maneuver are $\bar{u}_N = \text{atan}(\frac{\Delta\delta i_y}{\Delta\delta i_x})$ and $|x_N| = na\|\Delta\delta\boldsymbol{i}\|$, respectively [13]. In the presence of J_2, δi_y changes as a linear function of time as illustrated in Fig. 3. This leads to a combination of trigonometric and linear functions in the dynamics equation governing δi_y. Geometrically, the natural drift in δi_y before and after the maneuver must accumulate such that a single impulse provides the aimed change in relative inclination vector as derived from (12)

$$\cos(u_N)\, x_N = I\,, \tag{31}$$
$$[\sin(u_N) + \tfrac{\lambda}{N}(u_F - u_N)\cos(u_N)]\, x_N = J\,, \tag{32}$$

As a consequence, the location of the impulse is the solution of the following transcendental equation for which there is no analytical solution

$$\tan(u_N) + \tfrac{\lambda}{N}(u_F - u_N) = \tfrac{J}{I}\,. \tag{33}$$

However, the ideal solution $u_{N,ideal} = \text{atan}\left(\frac{\Delta\delta i_y}{\Delta\delta i_x}\right)$ for the unperturbed case can be used as a first guess to evaluate the effects of J_2 during the reconfiguration as shown in Table 4.

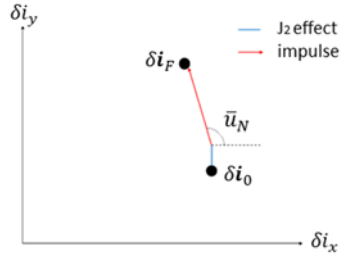

Figure 3. Effect of J_2 on relative inclination vector during reconfiguration

TABLE 4. OUT-OF-PLANE IMPULSE LOCATION IN NEAR-CIRCULAR ORBITS

J_2 effects included	Type of solution	Location of out-of-plane impulse
No	Analytical	$u_{N,ideal} = atan(\frac{J}{I})$
Yes	Numerical	$tan(u_N) + \frac{\lambda}{N}(u_F - u_N) = \frac{J}{I}$
Yes	Iterative / Quasi-analytical	Initialization: $tan(\tilde{u}_N) + \frac{\lambda}{N}(u_F - u_{ideal}) = \frac{J}{I}$ Iterations: $tan(\tilde{u}_N^+) + \frac{\lambda}{N}(u_F - \tilde{u}_N^-) = \frac{J}{I}$

This tentative maneuver location can be used to find an initial $\tilde{u}_N$ to be refined iteratively though a better approximation of the effects of J_2 at each iteration. In practice, only one iteration is sufficient. Once the location u_N has been computed, the corresponding delta-v is found using (33).

IV. CONTROL IN ECCENTRIC ORBITS

Fuel-optimal maneuvers in eccentric orbits have been addressed in literature using numerical optimization [10] or iterative optimal control algorithms [8]. In contrast, here closed-form solutions for fuel-optimal relative orbit control maneuvers are sought. In particular, an optimal semi-analytical solution is derived for reconfigurations characterized by $\|\Delta\delta\boldsymbol{e}\| > |\Delta\delta a^*|$. This directly extends previous work done in near-circular orbits.

A. Delta-v Lower Bound in Eccentric Orbits

This section addresses the delta-v lower bound in eccentric orbits which represents the absolute minimum required delta-v for any given reconfiguration. The most efficient maneuver direction for a given change in ROE can be found by comparing the normalized effects of a unit size delta-v on the ROE. From (15), the minimum radial burn for

a change in δa occurs at $\nu = \pi/2$ and its normalized effect is given by $\frac{2}{\eta}e$. Similarly, the minimum tangential burn for a change in δa occurs at $\nu = 0$ (i.e., at the perigee), where the velocity is maximum and tangent to the orbit. Its normalized effect is given by $\frac{2}{\eta}(1+e) > \frac{2}{\eta}e$. Therefore, the most efficient tangential burn is always smaller than the most efficient radial burn. As in near-circular orbits, the aimed $\delta\lambda'$ can be achieved through a tangential burn by introducing the drift coefficient for the appropriate duration of the reconfiguration. Equation (15) provides the normalized effect of an impulse on $\delta\boldsymbol{e}$ as well. The effect of a radial burn is constant and equal to η. The effect of a tangential burn is equal to $\eta\frac{\sqrt{(2+e\cos\nu)^2+e^2+2e(2+e\cos\nu)\cos\nu}}{1+e\cos\nu}$. The minimum of this function is equal to 2η at $\nu = k\pi$ (k integer). Thus, a tangential burn always has at least twice the effect on $\delta\boldsymbol{e}$ as compared with a radial burn. Based on these considerations, we can derive a delta-v lower bound for any given in-plane reconfiguration using tangential impulses. From (15), for a desired change $|\Delta\delta a|$, the minimum delta-v is given by

$$\left|x_{\mathrm{T,min}}\right|_{|\Delta\delta a|} = \frac{\eta}{2(1+e)}na|\Delta\delta a|. \tag{34}$$

The $|\delta a_{\mathrm{transf}}|$ needed to achieve an aimed $|\Delta\delta\lambda'|$ over a reconfiguration of duration $\Delta M_{\mathrm{reconf}}$ is given by

$$|\delta a_{\mathrm{transf}}| = \frac{2}{3\Delta M_{\mathrm{reconf}}}|\Delta\delta\lambda'|, \tag{35}$$

thus the minimum delta-v to achieve $|\Delta\delta\lambda'|$ is

$$\left|x_{\mathrm{T,min}}\right|_{|\Delta\delta\lambda|} = \frac{\eta}{3(1+e)\Delta M_{\mathrm{reconf}}}na|\Delta\delta\lambda'|. \tag{36}$$

Equivalently, for a change $\|\Delta\delta\boldsymbol{e}\|$ the minimum delta-v is found from (15) as

$$\left|x_{\mathrm{T,min}}\right|_{\|\Delta\delta\boldsymbol{e}\|} = \frac{1}{2\eta}na\|\Delta\delta\boldsymbol{e}\|. \tag{37}$$

Therefore, the delta-v lower bound for an in-plane reconfiguration in eccentric orbits is given by the $\left|x_{\mathrm{T,min}}\right|$ corresponding to the dominant desired change in ROE

$$\delta v_{\mathrm{LB}} = \max\left(\frac{\eta}{2(1+e)}na|\Delta\delta a^*|, \frac{1}{2\eta}na\|\Delta\delta\boldsymbol{e}\|\right) \tag{38}$$

where

$$|\Delta\delta a^*| = \max(|\delta a_F - \delta a_0|, |\delta a_F - \delta a_{\mathrm{transf}}|, |\delta a_{\mathrm{transf}} - \delta a_0|)\ ,$$

and $\delta a_{\mathrm{transf}}$ is given in (35). This newly derived delta-v lower bound is the direct extension to eccentric orbits of the lower bound given by (16) for near-circular orbits. In the latter case, $\eta \approx 1$, $e \approx 0$ and the expressions become identical.

B. In-Plane Reconfiguration

In accordance with the derivation above, we will try to find a closed-form solution to the reconfiguration problem using tangential burns only. A three-impulse maneuvering scheme guarantees enough degrees of freedom to achieve any aimed change in relative orbital elements and the dynamics equations are derived from (9) as

$$\begin{gathered}(1+e\cos\nu_1)x_{T1} + (1+e\cos\nu_2)x_{T2} + (1+e\cos\nu_3)x_{T3} = \eta A/2,\\ -3(1+e\cos\nu_1)(M_F - M_1)x_{T1} - 3(1+e\cos\nu_2)(M_F - M_2)x_{T2} - \\ 3(1+e\cos\nu_3)(M_F - M_3)x_{T3} = \eta L,\\ \frac{(2+e\cos\nu_1)\cos\theta_1 + e_x}{1+e\cos\nu_1}x_{T1} + \frac{(2+e\cos\nu_2)\cos\theta_2 + e_x}{1+e\cos\nu_2}x_{T2} + \frac{(2+e\cos\nu_3)\cos\theta_3 + e_x}{1+e\cos\nu_3}x_{T3} = \\ E/\eta - e_y J/\eta\tan i,\\ \frac{(2+e\cos\nu_1)\sin\theta_1 + e_y}{1+e\cos\nu_1}x_{T1} + \frac{(2+e\cos\nu_2)\sin\theta_2 + e_y}{1+e\cos\nu_2}x_{T2} + \frac{(2+e\cos\nu_3)\sin\theta_3 + e_y}{1+e\cos\nu_3}x_{T3} = \\ F/\eta + e_x J/\eta\tan i,\end{gathered} \tag{39}$$

An analytical solution for the three impulses is found by inverting the first three equations of (39)

$$x_{T1} = \frac{h_{23}}{K_{123}}, x_{T2} = \frac{-h_{13}}{K_{123}}, x_{T3} = \frac{h_{12}}{K_{123}}, \tag{40}$$

$$\begin{gathered}K_{ijk} = 6\eta\tan(i)[(M_i - M_j)f_i f_j g_k + (M_k - M_i)f_i f_k g_j + (M_j - M_k)f_j f_k g_i]\\ h_{ij} = 2L\eta^2(f_i g_j - f_j g_j) + 6(M_i - M_j)f_i f_j\,[E\tan(i) - Je_y]\\ +3A\eta^2\tan(i)\,[(M_F - M_i)f_i g_j - (M_F - M_j)f_j g_i]\\ f_i = 1 + e\cos(v_i)\\ g_i = [(1+f_i)\cos(\theta_i) + e_x]/f_i\end{gathered} \tag{41}$$

Equations (40-41) depend on the unknown locations of the three maneuvers. The locations that minimize the magnitude of the delta-v vector and satisfy the last of (39) can be found in the case that $\|\Delta\delta\boldsymbol{e}\|$ is dominant by ensuring a minimum path in ROE state-space as illustrated in Fig. 4. The control equations for the relative eccentricity vector are derived from (9) as

$$\frac{(2+e_x\cos\theta+e_y\sin\theta)\cos\theta+e_x}{1+e_x\cos\theta+e_y\sin\theta}x_T = E/\eta - e_y J/\eta\tan i\ , \tag{42}$$

$$\frac{(2+e_x\cos\theta+e_y\sin\theta)\sin\theta+e_y}{1+e_x\cos\theta+e_y\sin\theta}x_T = F/\eta + e_x J/\eta\tan i\ . \tag{43}$$

The ratio between (42) and (43) gives a relationship for the true arguments of latitude θ_i of the burns

$$tan\theta_i\,\frac{1+\frac{e_y}{(2+e_x\cos\theta_i+e_y\sin\theta_i)\sin\theta_i}}{1+\frac{e_x}{(2+e_x\cos\theta_i+e_y\sin\theta_i)\cos\theta_i}} = \frac{F\tan(i)+e_x J}{E\tan(i)-e_y J}. \tag{44}$$

Equation (44) can be solved numerically for the fuel-optimal maneuver locations. Good initial conditions for a numerical solver are the locations of the burns for near-circular orbits, $\theta_i = \mathrm{atan}\left(\frac{F}{E}\right) + k_i\pi$. The choice of integers k_i allows to select the maneuver locations among all the available solutions, thus simplifying the compliance with operational constraints.

C. Out-of-Plane Reconfiguration

The dynamics of an out-of-plane reconfiguration in eccentric orbits is derived from (9) as follows

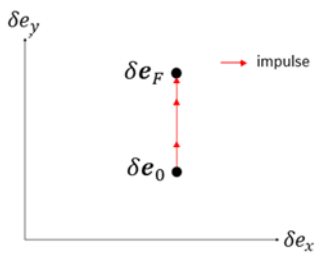

Figure 4. Optimal reconfiguration in $\delta e_x - \delta e_y$ plane

TABLE 5. IN-PLANE CONTROL SOLUTION IN ECCENTRIC ORBITS

Unknown	Type of solution	Solution
Locations θ_i	Numerical	$tan\theta_i \frac{1+\frac{e_y}{(2+e_x\cos\theta_i+e_y\sin\theta_i)\sin\theta_i}}{1+\frac{e_x}{(2+e_x\cos\theta_i+e_y\sin\theta_i)\cos\theta_i}} = \frac{F\tan(i)+e_xJ}{E\tan(i)-e_yJ}$
Magnitudes x_{Ti}	Analytical	$x_{T1}=\frac{h_{23}}{K_{123}}, x_{T2}=\frac{-h_{13}}{K_{123}}, x_{T3}=\frac{h_{12}}{K_{123}}$

TABLE 6. OUT-OF-PLANE CONTROL SOLUTION IN ECCENTRIC ORBITS

Unknown	Type of solution	Solution
Location θ_N	Analytical	$\theta_N = \text{atan}\left(\frac{J}{I}\right)$
Magnitude x_N	Analytical	$x_N = \frac{1+e\cos\nu_N}{\eta\cos\theta_N} I$ $or\ x_N = \frac{1+e\cos\nu_N}{\eta\sin\theta_N} J$

$$\eta x_N \tfrac{\cos\theta}{1+e\cos\nu} = I \quad (45)$$

$$\eta x_N \tfrac{\sin\theta}{1+e\cos\nu} = J \quad (46)$$

One cross-track delta-v is necessary and sufficient to satisfy the aimed end-conditions. By looking at the ratio between (45) and (46), the location of the normal impulse is given by

$$\tan(\theta_N) = \tfrac{J}{I}\ or\ \theta_N = \text{atan}\left(\tfrac{J}{I}\right) + k\pi. \quad (47)$$

The integer k has to be chosen so to minimize x_N, or equivalently to minimize $(1 + e\cos\nu_N)$. From its definition, $\nu_N = \text{atan}\left(\frac{J}{I}\right) - \omega + k\pi$, it is found that k has to be odd if $\cos\left[\text{atan}\left(\frac{J}{I}\right) - \omega\right] > 0$, or even in the other cases. Such a choice ensures that the relative inclination vector is changed in the proper direction. The magnitude of the impulse can be computed from (45-46).

V. NUMERICAL SIMULATIONS

This paper has derived a number of (semi-)analytical fuel-optimal impulsive control schemes which are numerically validated in this section. Extensive simulations have been carried out on a number of reconfigurations. The numerical simulation scheme is illustrated in Fig. 5. The maneuver's size and location are computed from the mean initial ROE and from the desired target ROE at the end of the reconfiguration. A numerical integration of the equations of motion is performed for each spacecraft orbit in osculating space by applying the impulsive maneuvers as discontinuities of the deputy's velocity. At the end of the propagation, a comparison is made between the achieved and desired mean ROE to evaluate functionality and performance. In addition, the reconfiguration results obtained from the closed-form solutions are compared with an optimal control algorithm designed by Roscoe et al. [8] as illustrated in Fig. 6. Based on Pontryagin's optimal control theory, it iteratively solves the discrete-time optimal control problem and refines the solution as from Lawden's primer vector theory. This is done by adding, removing, or moving impulsive maneuvers so to converge towards the continuous-time optimal solution. Although the output of this algorithm is the truly optimal impulsive maneuver, it suffers from complexity, poor convergence properties, computational effort, and is only used as a reference for comparison in the following.

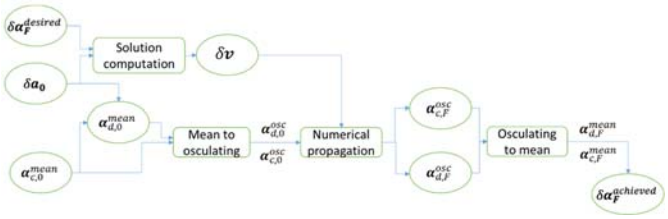

Figure 5. Diagram of the numerical simulation scheme

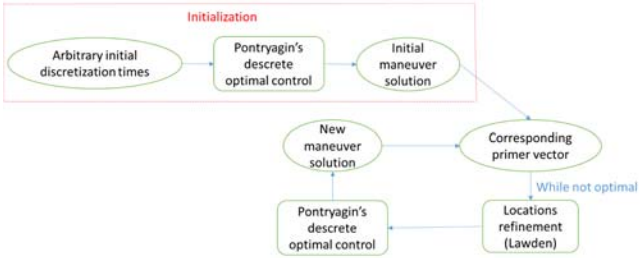

Figure 6. Optimal control algorithm

A. In-Plane Control in Perturbed Near-Circular Orbits

As a first step, we use an example reconfiguration to compare the closed-form control solutions (Tables 2-3) in the presence or absence of perturbations. The example in-plane reconfiguration requires a transfer from $a\delta\boldsymbol{\alpha}_0 = [50, -10000, 230, -50]$ m to $a\delta\boldsymbol{\alpha}_F = [0, -9800, 150, 0]$ m, within a time frame of 7.5 orbits. This corresponds to a reconfiguration where all the in-plane ROE are affected with a dominant change in the relative eccentricity vector. The reference orbit is circular at an altitude of 750 km.

TABLE 7. IN-PLANE ROE RECONFIGURATION ERROR

ROE	No perturbation	Perturbations included
$a\delta a$	0.005%	0.005%
$a\delta\lambda$	0.8%	0.347%
$a\delta e_x$	1.5%	0.14%
$a\delta e_y$	5.4%	0.468%

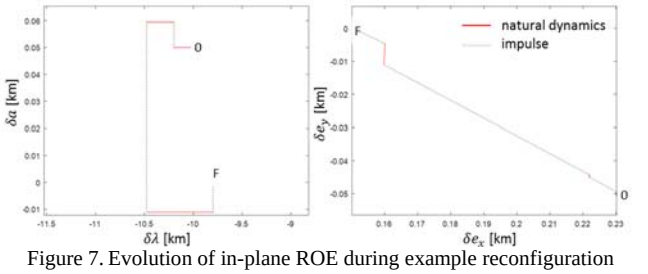

Figure 7. Evolution of in-plane ROE during example reconfiguration

The evolution of the in-plane ROE is shown in Fig. 7 where start and end states are tagged with 0 and F respectively. Note the rotation of the eccentricity vector between the burns. The accuracy of the reconfiguration for each in-plane ROE is listed in Table 7. The gain in reconfiguration accuracy is evident when the perturbations are included in the closed-form control solution. Figure 8 shows the behavior of the truly optimal solution from primer vector theory. The location of the impulses computed by the closed-form solution are indicated by red circles in Fig. 8. The optimum control algorithm gives multiple solutions corresponding to the peaks of the primer vector separated by half orbit period as expected from the closed-form solution. The indicated closed-form results correspond to a maximum of the primer vector with an arbitrary choice of $k_i = 0,1,14$ from (24). In contrast with the

optimal control approach, the closed-form approach allows for a convenient choice of k_i to eventually comply with operational constraints.

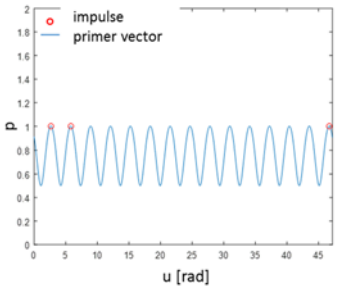

Figure 8. Impulse locations from closed-form and primer vector

Extensive simulations were run to systematically compare the delta-v outputs from the closed-form and optimal control methods. Fig. 9-10 show such comparisons in terms of absolute delta-v (in cm/s) and the relative difference (in %). Fig. 9 shows the case where the dominant change is $\|\Delta\delta\boldsymbol{e}\|$, which is used as independent variable with constant $|\Delta\delta a| = 0$. As expected, the required delta-v is proportional to $\|\Delta\delta\boldsymbol{e}\|$ (Fig. 9, left) and the closed-form solution gives the same delta-v as from the optimal control (Fig. 9, right). Indeed, the delta-v from the closed-form solution is slightly lower (~0.5%) in average than the optimal control output. This illustrates the fact that the iterative optimal control algorithm has convergence deficiencies. Fig. 10 shows simulation results where $a\|\Delta\delta\boldsymbol{e}\| = 100$ m and $|\Delta\delta a|$ varies as independent variable. As expected, as long as $|\Delta\delta a| < \|\Delta\delta\boldsymbol{e}\|$, the required delta-v is constant ($\|\Delta\delta\boldsymbol{e}\|$ is constant, Fig. 10, left) and the closed-form solution is optimal (Fig. 10, right). For $|\Delta\delta a| > \|\Delta\delta\boldsymbol{e}\|$, the delta-v results proportional to $|\Delta\delta a|$ and the closed-form solution is sub-optimal. In particular, the analytical delta-v is larger than the optimal delta-v by an offset of 7%. A new closed-form solution needs to be derived for this case. As from Fig. 1, a sufficient condition for optimality is that all the delta-vs have the same sign, so that the change $|\Delta\delta a|$ is covered by arrows of the same direction.

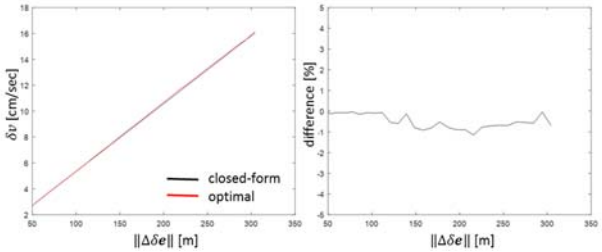

Figure 9. Optimality of in-plane solution when $|\Delta\delta a| < \|\Delta\delta e\|$

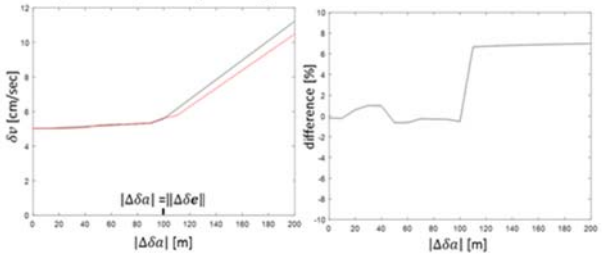

Figure 10. Optimality of in-plane solution when $|\Delta\delta a| > \|\Delta\delta e\|$

TABLE 8. OUT-OF-PLANE ROE RECONFIGURATION ERROR

ROE	No perturbation	Perturbations included
$a\delta i_x$	0.11%	0.10%
$a\delta i_y$	0.77%	0.34%

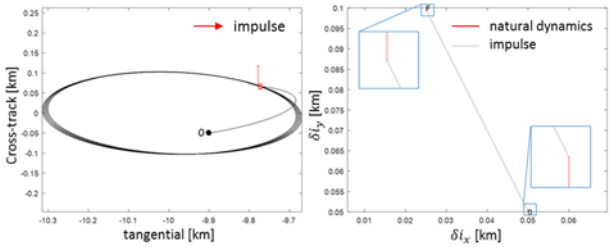

Figure 11. Relative motion in T-N plane (left) and ROE space (right)

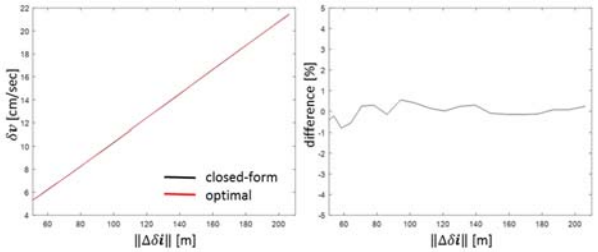

Figure 12. Optimality of out-of-plane solution

B. *Out-of-Plane Control in Perturbed Near-Circular Orbits*

The example reconfiguration used for out-of-plane control transfers the formation from $a\delta\boldsymbol{i}_0 = [50,50]$ m to $a\delta\boldsymbol{i}_F = [25,100]$ m over 7.5 orbits. Figure 11 shows the satellite relative motion in the T-N plane of the Hill's frame as well as the evolution of $\delta\boldsymbol{i}$ during the reconfiguration. Table 8 lists the reconfiguration errors by comparing actual and aimed $\delta\boldsymbol{i}$. Similar to Section V.A, the closed-form solution is validated by comparing the delta-v output with the optimal control algorithm. Fig. 12 shows such comparison for different values of $\|\Delta\delta\boldsymbol{i}\|$. As expected, the cost is proportional to the change in ROE and the analytical delta-v never exceeds the optimal value by more than 0.4%.

C. *In-Plane Control in unperturbed Eccentric Orbits*

The example reconfiguration is the same used in Section V.A, however the reference eccentricity is increased to 0.2. Here, no perturbations are included, so that the closed-form solution described in IV.B can be tested. Fig. 13 shows the in-plane ROE during the reconfiguration. The optimality of the solution is evident from the fact that the relative eccentricity vector moves along the shortest path from the initial to the aimed end-condition. As expected, the locations of the closed-form maneuvers occur at the maxima of the primer vector. The initial locations of the maneuvers were computed from $\theta_i = \text{atan}(F/E) + k_i\pi$ with $k_i = 0, 1, 14$.

For completeness, Fig. 14-15 show the reconfiguration results for an orbit eccentricity of 0.6. In the case $\frac{\eta}{(1+e)}|\Delta\delta a| < \frac{1}{\eta}\|\Delta\delta\boldsymbol{e}\|$ (Fig. 14), the closed-form solution is fuel-optimal and the required delta-v is proportional to $\|\Delta\delta\boldsymbol{e}\|$. Similar to the near-circular case, the analytical delta-v is slightly lower than the one from optimal control theory. In Fig. 15 ($a\|\Delta\delta\boldsymbol{e}\| = 100$ m), the closed-form solution is shown to be optimal as long as $\frac{\eta}{(1+e)}|\Delta\delta a| < \frac{1}{\eta}\|\Delta\delta\boldsymbol{e}\|$. After this threshold, the required delta-v becomes proportional to $|\Delta\delta a|$ and the closed-form solution is sub-optimal. An analytical optimal solution for this case remains to be found. This result is in agreement with the

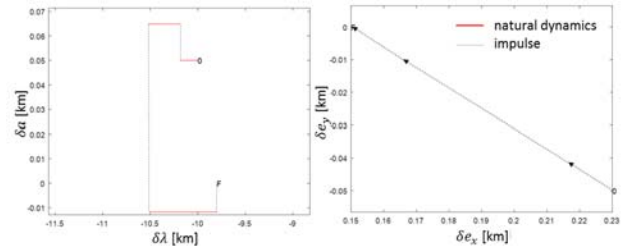

Figure 13. Evolution of in-plane ROE for eccentric orbits

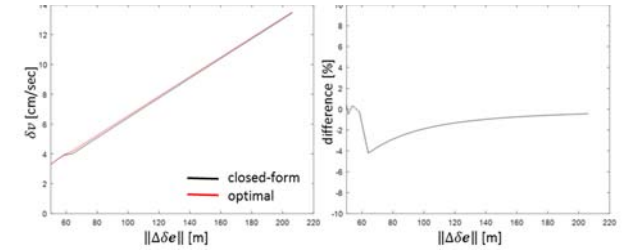

Figure 14. Optimality of in-plane solution when $\frac{\eta^2}{(1+e)}|\Delta\delta a| < \|\Delta\delta e\|$

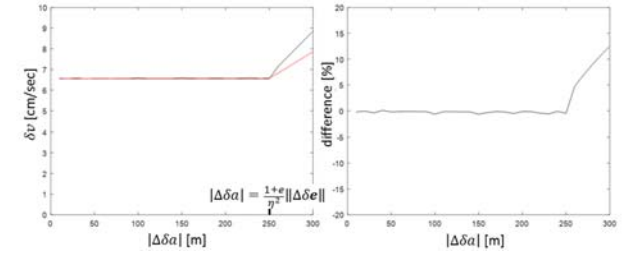

Figure 15. Optimality of in-plane solution when $\frac{\eta^2}{(1+e)}|\Delta\delta a| > \|\Delta\delta e\|$

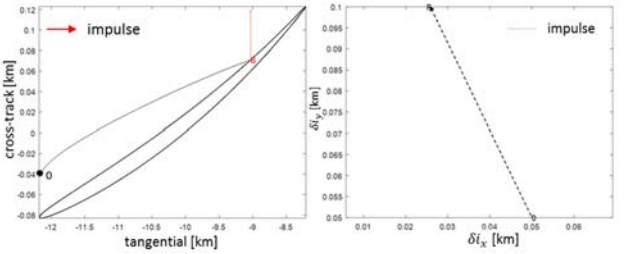

Figure 16. Relative motion in T-N plane (left) and ROE space (right)

derivation of the delta-v lower bound for eccentric orbits which predicts the switch in the change of ROE that drives the fuel-cost to be at $\frac{\eta}{(1+e)}|\Delta\delta a| = \frac{1}{\eta}\|\Delta\delta \boldsymbol{e}\|$.

Out-of-plane control in eccentric orbits is tested using the example reconfiguration of Section V.B., however the orbit eccentricity has been increased to 0.2. Fig. 16 shows the relative motion in the T-N plane of the Hill frame and the evolution of $\delta \boldsymbol{i}$ during the reconfiguration. The single impulse described in Section IV.C transfers the formation from start to aimed conditions according to a minimum path length in ROE state-space.

VI. Conclusion

This paper addressed the problem of closed-form optimal spacecraft formation control using impulsive maneuvers. First, a new simple method to derive the state transition matrix for mean ROE in perturbed orbits of arbitrary eccentricity was shown together with a generalized delta-v lower bound. Second, new in-plane and out-of-plane closed-form solutions for formation control were derived, namely in J_2-perturbed near-circular orbits and unperturbed eccentric orbits. The optimality of the solutions were numerically verified by comparing the costs achieved by the closed-form solutions with an optimal control algorithm based on primer vector theory. The results show that closed-form maneuver strategies have the potential to outperform optimal control methods in terms of computational effort, simplicity, and predictability. On the other hand, research efforts are necessary to overcome the encountered limitations. In particular, optimal analytical solutions for the cases of perturbed eccentric orbits and reconfigurations with large relative semi-major axis are missing. Future work will also focus on the fusion of closed-form and optical control methods to efficiently handle more challenging scenarios.

References

[1] D'Amico, S., Pavone, M., Saraf, S., Alhussien, A., Al-Saud, T., Buchman, S., Byer, R., Farhat, C., "Miniaturized Autonomous Distributed Space System for Future Science and Exploration", 8th International Workshop on Satellite Constellations and Formation Flying, 2015, 8-10 June, Delft University of Technology (2015).

[2] D'Amico, S., Ardaens, J.-S., Larsson, R., "Spaceborne Autonomous Formation-Flying Experiment on the PRISMA Mission", *AIAA Journal of Guidance, Control, and Dynamics*, vol.35, no.3, 834-850 (2012).

[3] Ardaens, J.-S., D'Amico, S., "Spaceborne Autonomous Relative Control System for Dual Satellite Formations", *AIAA Journal of Guidance, Control and Dynamics*, vol.32, no.6, 1859-1870 (2009).

[4] Ardaens, J.-S., D'Amico, S., and Sommer, J., "GPS Navigation System for Challenging Close-Proximity Formation-Flight", 24th International Symposium on Spaceflight Dynamics, 5-9 May 2014, Laurel, USA (2014).

[5] Gaias, G., Ardaens, J.-S., and D'Amico, S., "The Autonomous Vision Approach Navigation and Target Identification (AVANTI) Experiment: Objectives and Design", ESA GNC 2014, 9th International ESA Conference on GN&C Systems, 2-6 June 2014, Oporto, Portugal (2014).

[6] Tillerson, M., Inalhan, G., and How, J., "Co-Ordination and Control of Distributed Spacecraft Systems Using Convex Optimization Techniques," International Journal of Robust Nonlinear Control, Vol. 12, Nos. 2–3, 2002, pp. 207–242.

[7] Tillerson, M., and How, J., "Advanced Guidance Algorithms for Spacecraft Formation-Keeping," Proceedings of the American Control Conference, Vol. 4, 2002, pp. 2830–2835.

[8] Roscoe, C.W.T., Westphal, J.J., Griesbach, J.D. and Schaub, H., "Formation Establishment and Reconfiguration Using Differential Elements in *J*2-Perturbed Orbits," Aerospace Conference, IEEE, 2014.

[9] Lawden, D. F., *Optimal Trajectories for Space Navigation*, 1963.

[10] Rogers, A., Woosley, and McGwier, R., "Nonlinear Tracking of Optimal Maneuvers in Spacecraft Formations,", American Control Conference, IEEE, 2015.

[11] Schaub, H., and Alfriend, K. T., "Impulsive Feedback Control to Establish Specific Mean Orbit Elements of Spacecraft Formations," Journal of Guidance, Control, and Dynamics, Vol. 24, No. 4, (2001), pp. 739–745.

[12] Schaub, H., "Relative Orbit Control Methods," *Analytical Mechanics of Space Systems*, edited by AIAA Education Series.

[13] Gaias, G. and D'Amico, S., "Impulsive Maneuvers for Formation Reconfiguration Using Relative Orbital Elements," *Journal of Guidance, Control, and Dynamics*, Vol. 38, No. 6 (2015), pp. 1036-1049.

[14] Gaias, G., D'Amico, S. and Ardaens, J.-S., "Generalized Multi-Impulsive Maneuvers for Optimum Spacecraft Rendezvous in Near-Circular Orbit", *International Journal of Space Science and Engineering*, vol.3, no.1, pp. 68 - 88 (2015).

[15] D'Amico, S., Montenbruck, O., "Proximity Operations of Formation Flying Spacecraft using an Eccentricity/Inclination Vector Separation", *AIAA Journal of Guidance, Control and Dynamics*, vol. 29, no. 3, 554-563 (2006).

[16] Vaddi, S.S., Alfriend, K.T., Vadali, S.R. and Sengupta P., "Formation Establishment and Reconfiguration Using Impulsive Control", *Journal of Guidance, Control, and Dynamics*, vol. 28, no. 2, pp. 262-268 (2005).

[17] Alfriend, K.T., H. Yan," Evaluation and Comparison of Relative Motion Theories", *AIAA Journal of Guidance, Control, and Dynamics*,vol. 28, no. 2, pp. 254-261 (2005).

[18] Gaias, G, Ardaens, J.-S., Montenbruck, O., "Model of J2 Perturbed Satellite Relative Motion with Time-Varying Differential Drag", *Celest Mech Dyn Astr*, Published Online on 19 August, 2015.

[19] Sullivan J., Koenig A., D'Amico S., "Improved Maneuver-Free Approach to Angles-Only Navigation for Space Rendezvous", 26th AAS/AIAA Space Flight Mechanics Meeting, Napa, CA, February 14-18, 2016.